

Implementation of an Electromagnetic Tracking System for Accurate Intrahepatic Puncture Needle Guidance: Accuracy Results in an In Vitro Model¹

Elliot B. Levy, MD, Jonathan Tang, BS, David Lindisch, RT, Neil Glossop, PhD, Filip Banovac, MD, Kevin Cleary, PhD

Rationale and Objectives. Electromagnetic tracking potentially may be used to guide percutaneous needle-based interventional procedures. The accuracy of electromagnetic guided-needle puncture procedures has not been specifically characterized. This article reports the functional accuracy of a needle guidance system featuring real-time tracking of respiratory-related target motion.

Materials and Methods. A needle puncture algorithm based on a “free-hand” needle puncture technique for percutaneous intrahepatic portocaval systemic shunt was employed. Preoperatively obtained computed tomographic images were displayed on a graphical user interface and registered with the electromagnetically tracked needle position. The system and procedure was tested on an abdominal torso phantom containing a liver model mounted on a motor-driven platform to simulate respiratory excursion. The liver model featured two hollow tubes to simulate intrahepatic vessels. Registration and respiratory motion tracking was performed using four skin fiducials and a needle fiducial within the liver. Success rates for 15 attempts at simultaneous puncture of the two “vessels” of different luminal diameters guided by the electromagnetic tracking system were recorded.

Results. Successful “vessel” puncture occurred in 0%, 33%, and 53% of attempts for 3-, 5-, and 7-mm diameter “vessels,” respectively. Using a two-dimensional accuracy prediction analysis, predicted accuracy exceeded actual puncture accuracy by 25%–35% for all vessel diameters. Accuracy outcome improved when depth-only errors were omitted from the analysis.

Conclusions. Actual puncture success rate approximates predicted rates for target vessels 5 mm in diameter or greater when depth errors are excluded. Greater accuracy for smaller diameter vessels would be desirable for implementation in a broader range of clinical applications.

Key Words. Electromagnetic tracking; abdominal phantom; liver interventions; image guidance.

© AUR, 2007

Accurate placement of needles within the liver for percutaneous interventions may be accomplished using computed tomography (CT), magnetic resonance imaging (MRI), or ultrasound guidance. Modality-specific limitations include requiring ionizing radiation, nonmagnetically susceptible instruments, or adequate acoustical window without interposed osseous or gas-filled structures. In more complex intrahepatic vascular procedures such as transjugular intrahepatic portocaval systemic shunt (TIPS), shunt creation between portal and hepatic veins is most often accomplished without direct real-time guidance, although planar and three-dimensional ultrasound (1,2) and MRI guidance has been reported (3). Alternatively, the target portal vein can be identified fluoroscopically.

Acad Radiol 2007; 14:344–354

¹ From the Department of Radiology, Section of Interventional Radiology (E.B.L., F.B.) and Imaging Sciences and Information Systems Center (J.T., D.L., F.B., K.C.), Medstar-Georgetown University Hospital, 3800 Reservoir Road, NW, Washington, DC 20007; Traxtal Technologies, Bellaire, TX (N.G.). E.B.L., F.B., and K.C. hold a patent for the Graphical User Interface software. Neil Glossop works for Traxtal Technologies, the developer of the MagTrax needle. Received June 9, 2006; accepted December 8, 2006. Supported by an Academic Transition Award from the Cardiovascular and Interventional Radiology Research and Education Foundation, 2001 (E.L.), and U.S. Army grant DAMD 17-99-1-9022 (K.C.). **Address correspondence to:** E.B.L. e-mail: levye@gunet.georgetown.edu

© AUR, 2007

doi:10.1016/j.acra.2006.12.004

cally by several techniques, including wedged hepatic venography using iodinated contrast or carbon dioxide (4), transhepatic portography, or percutaneous placement of target guidewires or markers in the portal vein (5,6).

Respiratory motion interferes with accurate needle placement in static CT-guided interventions, although real-time imaging with ultrasound, CT fluoroscopy, or MRI with breath-hold can help compensate for target excursion with respirations. In an alternative approach, static images would be registered with positional data obtained from an electromagnetic tracking system, allowing the position of electromagnetically tracked instruments to be displayed on the static image. Electromagnetic tracking could be enhanced to track the respiratory related motion of the target organ with retrievable embedded fiducials. The electromagnetic tracking system would then provide 1) real-time location of the tracked needle or instrument and 2) real-time location of the target during the respiratory cycle-related target excursion.

Electromagnetic sensors and tracking technology have found numerous applications in medicine, including surgical simulation and training and biomechanical analysis. Real-time motion can be captured in terms of (x,y,z) translation coordinates and (y,p,r) yaw, pitch, and roll coordinates, respectively (7). A complete tracking system typically consists of an electromagnetic field generator, sensors, and an interface device that communicates sensor data to a computer. Electromagnetic tracking as a guidance system for interventional procedures offers several advantages, including the lack of a requirement for ionizing radiation, high data sampling rates, and no line-of-sight interference issues. Electromagnetic tracking alone cannot display data in image form and must be registered with a specific image volume to function as an intervention guidance system. Electromagnetic tracking systems are additionally limited by field distortion caused by nearby metallic or electronic devices, diminished positional accuracy at increased distances from the field generator, and, to a lesser extent, positional display latency.

Recently, an interactive image guidance system featuring electromagnetic tracking coupled to previously acquired three-dimensional CT images was used to display the real-time position of the intrahepatic puncture needle during TIPS in a swine model (8). This system featured respiratory gating consisting of an electromagnetic sensor placed on the animal's abdomen, allowing updating of the needle position only during a designated portion of the respiratory cycle. This algorithm required the placement of 10–20 metallic markers on the animal's skin to permit

image registration. The system accuracy was reported to be 3 mm.

In this article, we report our preliminary accuracy results with an electromagnetic tracking system featuring real-time monitoring of respiratory-related target organ motion by a percutaneously placed retrievable fiducial. We also have selected the creation of an intrahepatic portosystemic shunt as our procedural model because the successful simultaneous puncture of two vessels demands a higher degree of accuracy in the performance of multiple steps in the procedure; the needle puncture path and specifically the puncture entry site is necessarily constrained by the alignment and diameter of the two vessels as well as the presence of interpositioned organs. By comparison, successful targeting of a single nodule simulating a simple biopsy can be achieved despite significant surface puncture site selection error. Although the presence of ascites might preclude the percutaneous transhepatic approach for routine application, electromagnetic tracking-guided percutaneous intrahepatic portocaval systemic shunt (PIPS) might be an alternative to TIPS if jugular access could not be achieved.

Our strategy for needle placement and manipulation for PIPS is patterned after the stepwise conventional "free-hand" procedure for static image-guided needle biopsies, but the puncture of the hepatic and portal veins would be performed percutaneously instead of a transjugular approach. Such an approach for intrahepatic portocaval systemic shunt may be technically feasible in up to 75% of patients (9). The role of the electromagnetic tracking guidance algorithm would be to enhance the accuracy of the transhepatic needle puncture and reduce the number of puncture attempts required for success.

In the electromagnetic tracking-guided needle puncture algorithm, puncture site and trajectory planning are determined with the assistance of a graphical user interface (GUI), a single intrahepatic fiducial needle, and a preoperatively obtained CT dataset. In our model, the CT dataset would be obtained at end-expiration in the animal model by suspending mechanical ventilation of the animal and allowing complete exhalation of the respiratory tidal volume to occur. Although mechanical ventilation would continue throughout the puncture procedure, guided needle advancement would be performed only when the internal tracked needle fiducial and GUI indicate that respiratory-related organ motion has ceased during the typically observed approximately 1.4 seconds regular end-expiratory phase pause (10). At this point, the actual alignment of the selected skin puncture site and intrahe-

patic targets will most closely approximate the predetermined puncture trajectory.

During the needle puncture procedure, the GUI also displays in separate windows the alignment of the puncture needle relative to the selected trajectory and the position of the needle tip superimposed on the preoperative planning CT image and the depth of the needle tip relative to the target depth in diagrammatic fashion. The operator is guided to correctly position the needle for successful puncture at end-exhalation by a separate window, which graphically displays the alignment of the hub of the needle with the target in the form of two circles that appear to overlap when the needle is properly aligned according to the planned puncture trajectory. The needle procedure can therefore be terminated by the operator based on the real-time information and guidance provided by the GUI.

MATERIALS AND METHODS

Determination of Positional Accuracy of the Tracking System

The Aurora Electromagnetic Tracking System includes of a small pyramidal electromagnetic field generator, a system control unit, and one or more sensor interface units. Initially, electromagnetically tracked sensors consisting of a single 0.9-mm diameter coil were embedded in a 5F standard straight polytetraethylene catheter and the tip of the stylet of a modified 18-gauge trocar needle (MagTrax needle, Traxtal Technologies, Bellaire, TX).

The positional accuracy of the Aurora system was initially evaluated in the absence of ferromagnetic interference in a nonclinical environment. A MagTrax 18G needle containing a single 5 degrees of freedom (DOF) electromagnetically tracked sensor was solidly fixed to two passive optically tracked rigid bodies (one small 50×50 mm body and one large 95×95 mm body to create a single sensor assembly). The optical sensing system is highly accurate and considered to provide "ground truth" in this comparison. The fixed electromagnetic/optical sensor assembly was moved randomly through 101 positions in a volume of $36 \text{ mm} \times 36 \text{ mm} \times 47 \text{ mm}$. At each location, the sensor assembly was fixed in position and 10 samples from each of the targets were collected by the Polaris optical system (Northern Digital Inc, Ontario, Canada) and Aurora electromagnetic system (Northern Digital, Inc). The datasets were aligned by least-square point set-to-point set registration and the differences in

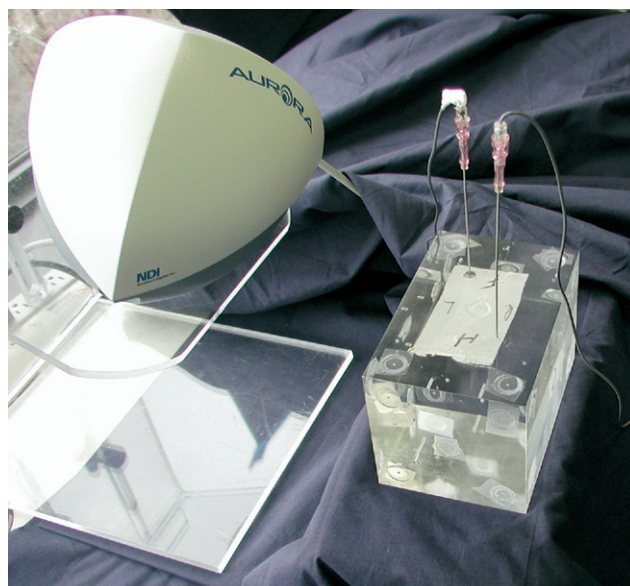


Figure 1. Electromagnetic field generator and tracked needles with phantom for fiducial localization error measurements.

position and orientation of the two Polaris optical sensors (control) versus the Magtrax electromagnetically tracked probe were calculated over the 101 positions.

Positional accuracy assessment was then repeated in a Neurostar T.O.P. Polytron interventional radiology suite (Siemens Corp, Erlangen, Germany) to test for possible electromagnetic field disturbance and positional data inaccuracy from large adjacent metallic structures such as the procedure table and C-arm image intensifier x-ray source combination. The PAKY/remote center of motion needle driver robot (11) designed for interventional procedures was mounted directly on the procedure table in the interventional suite to serve as a needle holder and precision positioning device (Fig 1). The robot consists of a translation stage with 3 DOF, a 7 DOF passive positioning stage, and a 3 DOF orientation/driving stage that can be precisely positioned according to specified coordinates. Positioning and robotic arm excursion distances were checked and confirmed for accuracy with the Polaris optical tracking system. The passive positioning stage, which is used for the initial gross positioning of the needle in clinical applications, has similar kinematics to the human arm and consists of a three DOF shoulder, a one DOF elbow, and a three DOF wrist. A MagTrax 18G needle "grasped" and positioned by the robot was electromagnetically tracked at seven locations over a $100 \text{ mm} \times 40 \text{ mm} \times 40 \text{ mm}$ volume. The distances between the seven locations were determined by the differences in root mean

square calculations between successive points. The seven different locations were surveyed a total of seven times, and displacement determined by comparing magnetic coordinates and robot-controlled displacement distances (mean, standard deviation). The reference axis of motion was defined by the coordinate system of the robotic device.

Determination of Orientation Accuracy of the Tracking System

For orientation accuracy, a MagTrax needle was affixed to the robotic arm at the remote center of motion point, and the robot was programmed to position the MagTrax needle at eight different positions within a 10 mm × 10 mm × 10 mm cubic test volume. At each position, the MagTrax needle was then oriented from -30° to 30° in 10° increments. Coordinate data were recorded and expressed as means and standard deviations.

Accurate Measurement of the Coil Offset

To accurately register the tip of the needle used as the internal fiducial, the distance from the tip to the centroid of the coil must be known and the electromagnetic positional data for the needle tip (offset) adjusted accordingly.

To measure the accuracy in calculating the position of the probe tip, the PAKY/remote center of motion robot was programmed to pivot the electromagnetically tracked needle about its tip. This form of "pivot test" is routinely used for calculating offsets between tracked sensors and the tip of the localization probe (12). The offset for each needle can be similarly calculated from the position and orientation data collected in the pivot routine as a least squares function. Before the registration step in the needle puncture procedure, the GUI would prompt the user to enter the unique coil offset measurement for the particular needle in use. By applying the offset to the data returned by the Aurora system we are able to determine the precise position of the MagTrax needle for registration and tracking during the needle puncture experiments. The error in determining tip position was measured as the variance (standard deviation) in the calculated tip position during several robot-controlled pivot routines.

Phantom Design and Needle Puncture Procedure

An abdominal torso phantom (Anatomical Chart Co, Skokie, IL) was modified by removing the ventral abdominal wall and placing a servomotor-driven platform mount in the "paraspinal" area on which a liver phantom has

been secured. The liver phantom consists of a commercially produced processed turkey meat preparation (Jenny-O Turkey Store, Hormel Foods Corp, Austin, TX) in which channels serving as target "vascular structures" are created by drilling one to two pairs of 3-mm, 5-mm, or 7-mm diameter cores per phantom and injecting the resulting "tubes" with a mixture of barium sulfate (Eso-pho-cat 3% w/w, EZEM, Westbury, NY), iodinated contrast material (Omnipaque, Amersham Health, Cork, Ireland), and agarose gel (Agar, Fisher Scientific, Fair Lawn, NJ). The phantom is similar in firmness to the normal human liver with respect to the tactile sensation during needle puncture. The servomotor control system produces linear platform motion which simulates the craniocaudal respiratory motion of the liver.

In initial feasibility experiments, a single electromagnetically tracked coil was embedded in a 5F straight polytetraethylene catheter, which was then used as an internal fiducial to track the internal position of the liver model. However, it proved to be difficult to achieve stability of the catheter without resorting to strong adhesives, which then made reuse of catheters in additional experiments virtually impossible. Some difficulty identifying the centroid of the coil under fluoroscopy was also encountered which resulted in significantly larger registration errors. Therefore, an 18G MagTrax needle was embedded in the "cephalad" portion of liver phantom, which served as an internal fiducial to track phantom motion on the servomotor platform during simulated respiratory movement. The remaining four fiducials are calibrated flat skin markers (multimodality radiographics markers, IZI Medical, Baltimore, MD) placed on the anterior costal margins which can be readily identified on axial CT images of the torso. A second retMagTrax 18G needle served as the tracked puncture needle.

The servomotor platform set the liver phantom at the maximal "cephalad" point in the prescribed respiratory excursion range, corresponding to the point of "end-expiration" (home position). The phantom was placed in a Siemens CT scanner and contiguous 3mm images of the "liver" obtained with a 512×512 matrix, field of view 310 mm, and pixel size 0.36 mm^2 and reconstructed at 1-mm slice intervals.

The CT DICOM dataset was transferred to a Windows NT workstation for image review and target selection. A custom GUI permitted review of the CT dataset in axial, sagittal, and coronal reconstructed fashion as well as displaying in-plane and well as out-of-plane planned needle puncture paths. The GUI soft-

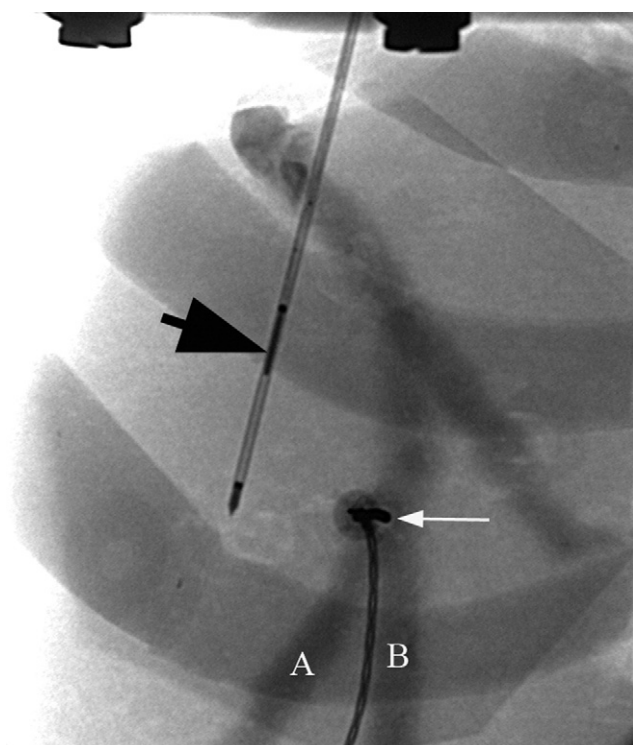


Figure 2. Frontal image demonstrating successful simultaneous puncture of both target vessels (A,B). Bold black arrow: needle fiducial; white arrow: puncture needle.

ware was developed using Visual C++. The Visualization Toolkit (VTK, Kitware, Inc, Clifton Park, NY) was used for visualization along with the Fast Light Toolkit (FLTK, www.fltk.org) for the user interface elements. Modules for importing the image data in DICOM format, visualization of reformatted slices, and identification of fiducials were included.

The target vessels were selected and a linear puncture needle trajectory highlighted. The electromagnetic field generator was placed next to the torso. Image and magnetic space registration was accomplished using a single needle-based internal fiducial and four skin fiducials. Registration of the skin fiducials was accomplished by identifying the fiducials on the CT images and placing the electromagnetically tracked puncture needle on the perceived isocenter of each fiducial sequentially, thereby recording the position of the fiducial in magnetic space. The internal needle-based fiducial was registered in the end-expiratory phase position by returning the servomotor platform to the “home” (end-expiratory) position and identifying the tip of the needle containing the coil fiducial on the respective CT image. In all experiments, the registration error (root

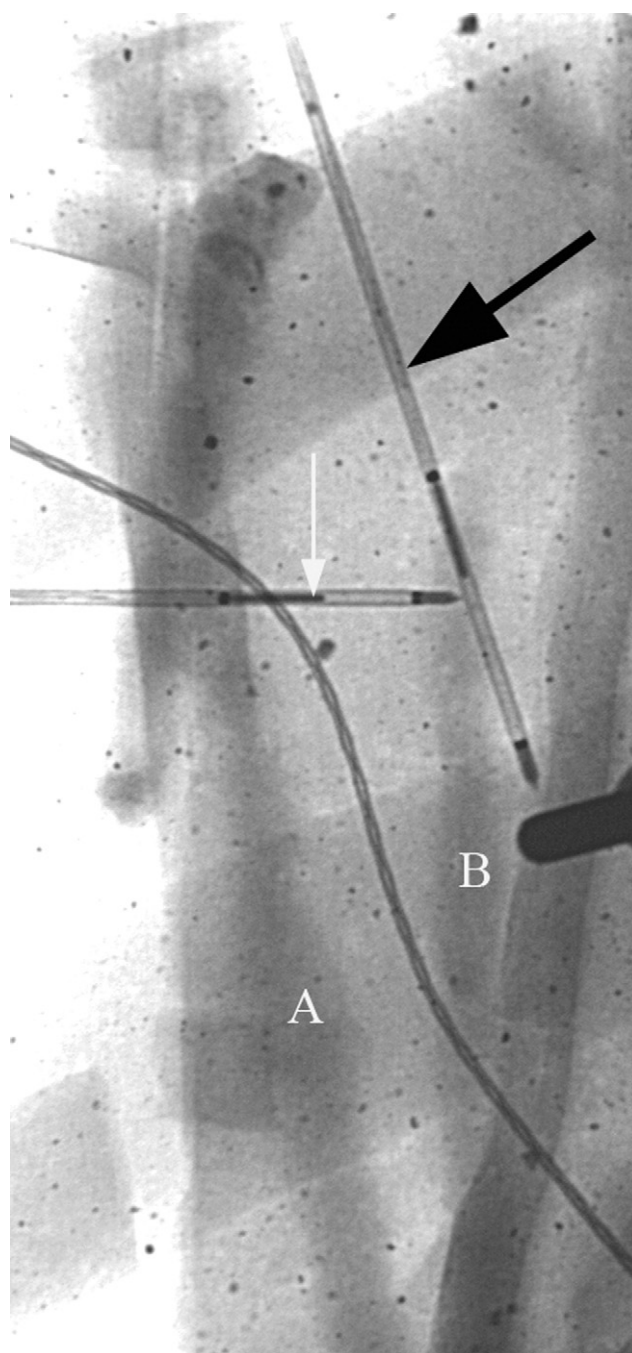


Figure 3. Lateral view of the same needle and target vessels. Bold black arrow: needle fiducial; white arrow: puncture needle.

mean square) measured 1–2 mm. The skin entry site was determined by placing the electromagnetically tracked needle on the “skin” of the torso where the tip of the needle intersected the previously determined needle puncture trajectory as displayed by the GUI. During puncture attempts, the projected needle tip

Table 1
Manufacturer's Specifications for the Aurora System

	Five-Dimensional Sensor
Accuracy positional	1–2 mm 3D root mean square*
Accuracy angular	0.5°–1° root mean square*
Sensor	
Dimensions	0.9 mm diameter × 8 mm
Number of sensors	1–10
Measurement rates	20–60 Hz†

Table courtesy of Northern Digital, Inc.

*Accuracy varies with sensor orientation.

†Independent of number of sensors tracked.

could be compared to the termination target position in real-time fashion, and needle advancement ceased when the system graphically indicated the desired needle depth had been achieved.

Each needle pass was timed, and determination of the final needle tip position determined by orthogonal digital fluoroscopic images of the phantom (Fig 2,3). A total of 15 needle passes were performed by a single operator (E.L.) experienced with image-guided needle puncture procedures on individual phantoms containing two vessels of identical diameter. Registration error was checked at least twice for each phantom during the 15 puncture attempts. Images were archived and converted from DICOM files to bitmap images using Angio-PC 4.0 (Siemens Corp). A pixels-to-millimeters conversion ratio was initially obtained for each pair of images by dividing the measured needle diameter in pixels using Adobe Photoshop by the 1.33-mm standard 18-gauge needle diameter. Images were subsequently reviewed to determine successful puncture attempts and errors.

Target errors occurred when one or both “vessels” were missed in the anteroposterior projection. Combinations of depth and target errors were also recorded. Puncture success was defined as 1) simultaneous puncture of the wall or lumen of both “vessels,” and 2) terminal position of the needle tip within the wall or lumen of the deeper “vessel.” Depth errors occurred when both target vessels were punctured but the deeper “vessel” was punctured through both walls or if the terminal position of the needle tip was superficial or deep to the deeper vessel. Actual puncture success was compared with predicted puncture accuracy for each vessel diameter using methodology described in the Appendix.

Table 2
Magnetically Measured Displacement by Robot Axis

x-axis	
0–100 mm	100.15 ± 0.10
100 mm to 0 mm	100.46 ± 0.58
y-axis	
0–20 mm	19.88 ± 0.10
20 mm to –20 mm	39.28 ± 0.02
–20 mm to 0 mm	19.43 ± 0.04
z-axis	
0–20 mm	19.99 ± 0.02
20 mm to –20 mm	40.06 ± 0.05

Table 3
Needle Puncture Experiment

	Incidence			Total
	3 mm	5 mm	7 mm	Frequency
Unsuccessful punctures				
Missed superficial vessel 1	1	2	1	4
Missed deep vessel 2	7	2		9
Missed both vessels	2			2
Depth error only		2	5	7
Missed vessel 1 + depth error	1			1
Missed vessel 2 + depth error	4	1	1	6
Missed vessels 1, 2 + depth error		3		3
Successful punctures	0	5	8	
Total passes	15	15	15	

RESULTS

Manufacturer's Stated System Accuracy

The manufacturer's specifications for the Aurora system are shown in Table 1.

Positional Accuracy

Using the optical passive tracking system as the gold standard as described in the Materials and Methods section, the mean measurement error and standard deviation of the MagTrax needle using the Aurora system was 0.71 ± 0.43 mm ($n = 101$) in a nonsurgical environment. The maximum error noted was 2.96 mm (13).

Table 2 compares actual MagTrax needle displacement with displacement distance determined by the Aurora electromagnetic tracking system with the robot-tracking system assembly placed upon the procedure table with the

Table 4
Predicted vs. Actual Puncture Error Analysis

All Puncture Attempts

Total Error (mm)	Vessel Diameter (mm)	Predicted Success Rates		Mean	Observed Success Rate	Difference	Total Attempts
		Perpendicular Case	Parallel Case				
4.23	3	0.16	0.42	0.29	0.00	0.29	15
4.23	5	0.44	0.63	0.54	0.30	0.24	15
4.23	7	0.86	0.89	0.88	0.53	0.35	15

All Puncture Attempts excluding Depth Errors

Total Error (mm)	Vessel Diameter (mm)	Predicted Success Rates		Mean	Observed Success Rate	Difference	Total Attempts
		Perpendicular Case	Parallel Case				
4.23	3	0.16	0.42	0.29	0.00	0.29	15
4.23	5	0.44	0.63	0.54	0.39	0.15	13
4.23	7	0.86	0.89	0.88	0.80	0.08	10

C-arm fluoroscopic unit parked in a neutral position away from the table (14).

Orientation Accuracy

In the worst case, the orientation error measured 0.70° , which would be equivalent to a targeting error of 1.22 mm for a 10-cm deep lesion (15).

Needle Puncture Experiments

The results of the needle puncture experiments are summarized in Tables 3 and 4. "Vessel 1" is defined as the more superficial of the two vessels, whereas "Vessel 2" is the deeper vessel. Guided needle placement was least successful in the smallest size vessels (0/15 successful two-vessel punctures in 3-mm diameter targets) and was most successful in the largest diameter targets (8/15 successful two-vessel punctures in 7-mm vessels).

The overall error, calculated as the sum of the maximum registration error, maximum targeting (orientation) error, and mean measurement error, was 4.23 mm. The average registration errors for the puncture procedures were 2.0, 2.3, and 2.2 mm for the 3-mm, 5-mm, and 7-mm diameter vessel targets, respectively.

Table 4 compares predicted mean and actual puncture success rates for each vessel diameter. Actual puncture success rates are significantly less than mean predicted rates for all diameters. When depth errors are removed, successful punctures occur for 5 mm and 7 mm diameter targets within 15% of predicted success rates.

DISCUSSION

Interactive image guidance has been implemented to improve intervention accuracy in several applications. In the neurosurgical theater, systems featuring optical and electromagnetic tracking have been used to simultaneously display the position of intraoperative instruments on preoperative image datasets. Optical tracking systems are limited by line-of-sight requirements for optical fiducial markers. Electromagnetic tracking systems do not have this limitation. Real-time electromagnetic tracking-based guidance systems supplemented with static images have been employed previously for the TIPS procedure (8) as well as bronchoscopy (16).

We selected the PIPS as our procedure model because 1) intrahepatic portocaval systemic shunt creation has become an important therapeutic procedure for the management of the complications of portal hypertension; 2) the essential step is also the most complex (ie, intrahepatic puncture of the hepatic and portal veins; 3) the intrahepatic puncture is most often performed in blind fashion; and 4) it might be possible to selectively and more confidently target the intrahepatic portions of the portal veins using the magnetic tracking-guided approach in selected patients. In contrast to the work of Solomon et al (8), we have elected to follow a more generic percutaneous guided needle placement paradigm. This needle guidance algorithm necessarily requires a modification of the conventional TIPS procedure in which the creation of the

intrahepatic shunt follows initial direct percutaneous transhepatic puncture of the portal and hepatic veins. A single instance of percutaneous transhepatic puncture of a portal vein branch terminating in the inferior vena cava for TIPS has been previously reported using CT guidance (17). In a review of prior abdominal CT scans in a small number of patients with cirrhosis, we previously determined that a safe percutaneous transhepatic access to a portal and hepatic vein branch for PIPS creation was present in at least 75% of the patients (9). Unlike the shunt created from the portal vein to the inferior vena cava, the placement of PIPS should not preclude liver transplantation.

The transcapsular puncture required for PIPS compares unfavorably with conventional TIPS because of the additional risk of intrahepatic or intraperitoneal hemorrhage, particularly in patients with significant ascites. Although hemorrhage risk would be reduced by using smaller caliber puncture needles and preprocedure paracentesis, balloon dilation of the intrahepatic track would require transjugular or transfemoral access to the percutaneously placed guidewire. The proposed procedure may provide an alternative approach in patients in whom the conventional transjugular approach using a Colapinto needle may not be feasible. The PIPS paradigm is still useful for testing and validating electromagnetic tracking guided hepatic puncture procedures compared with conventional nodule biopsy, for example, because a successful combined two-vessel target puncture is constrained by a smaller margin of tolerable error proportional to the diameter of the vessels themselves.

These preliminary experiments were conducted on an *in vitro* phantom to determine the feasibility of the needle puncture guidance algorithm and to assess the overall guidance system success rate relative to the size of the target vessels. Our results are expressed as a calculation of individual inherent system errors, a tally of successful sequential puncture attempts, and a comparison between predicted and achieved puncture success. In this analysis, "success" in terms of target puncture can be defined as proven puncture of the lumen of the more superficial target and terminal position of the needle tip within the lumen of the deeper target or exact placement of the needle tip at preselected image target coordinates. In the first case, this definition of "success" refers to the clinical efficacy of the system (ie, the ability to gain access to the targeted vessels in the simulated PIPS procedure and not the absolute accuracy of the system). This first definition provides the framework for the results reported in this

investigation. The second definition constitutes the absolute accuracy of the operator guided by the electromagnetic tracking system within this experimental framework.

This *in vitro* system relies on the accuracy of the CT imaging and electromagnetic tracking systems, as well as the integrity of the phantom itself. CT imaging systems have inherent image inaccuracy such as image reconstruction errors that cannot be corrected. The types of errors related to electromagnetic tracking and image registration can be generally divided into the categories of fiducial localization error, fiducial registration error, human manipulation error, and target registration error, with the latter representing inherent inaccuracy representing a target established with an image coordinate system in magnetic space.

We initially endeavored to categorize the inherent error in the Aurora electromagnetic localization system itself. The manufacturer reports a 1–2 mm three-dimensional root mean square (RMS) positional accuracy and a 0.5° – 1° (RMS) angular accuracy, although this accuracy may vary with sensor orientation. In preliminary experiments, we investigated the accuracy of the Aurora system in a benchtop comparison with an optical tracking system and in the interventional suite using a calibrated robot. Our observed mean positional error and standard deviation using the MagTrax needle and Aurora system of $0.71 \text{ mm} \pm 0.43 \text{ mm}$ ($n = 101$), with a maximum error was 2.96 mm (11) is highly suitable for *in vivo* testing. Similar accuracy was determined for displacement error magnitude.

Most image-guided systems report overall fiducial misalignment in the form of the fiducial registration error (18) represented by the root mean square error. Fiducial registration error represents the misalignment of coordinates of individual points in magnetic and CT spaces, respectively. We recalculated the registration error at random intervals during our puncture experiments, and detected a single instance of significantly greater registration error, which coincided with a larger vessel targeting error. This single needle pass was omitted from the analysis as the registration error had increased by 50%. The average registration error including all vessel diameters was $2.14 \pm 0.15 \text{ mm}$.

Fiducial localization error refers to the inherent difficulty selecting the precise point in image or magnetic space that accurately represents the individual fiducial. Similarly, misalignment of a selected target point from the registration process is called target registration error. In our system, fiducial localization errors are introduced

when each “skin” fiducial is localized by “tapping” the center of the fiducial marker visible on the CT images using an electromagnetically tracked needle and collecting the subsequent magnetic space coordinates. Slight error can be introduced by variations in the alignment of the needle or probe used to “tap” the fiducials, as well as in identifying the isocenter of the skin fiducials on the CT images. Similarly, some inaccuracy may arise in choosing the precise tip of the internal fiducial needle on the axial CT images. Each needle has a specific and unique “offset” that represents the distance from the needle tip to the reference point within the fiducial coil which must be entered into the calculation for the fiducial localization in CT space. The internal needle-based fiducial in the current design is also susceptible to displacement by the servomotor platform, multiple needle punctures, or operator error. The degree of fiducial registration error arising from needle displacement or fiducial localization inaccuracy was assessed by performing registration with five fiducials (four skin fiducials and one internal fiducial), after which registration was recalculated using only four of the fiducials selected at random. The error (RMS) was then calculated for the registration using the four selected fiducials. In almost every case, the greatest contribution to registration error arose from the internal fiducial. Increased registration errors related to fiducial motion could also be expected from movement of skin fiducials on animal or human subjects.

The described in vitro testbed clearly has significant limitations for evaluating electromagnetic tracking-guided interventions. The present phantom cannot replicate identically the internal architecture of the human liver, nor does the processed meat product exhibit the same tactile feedback or motion with respect to direct needle puncture. Degradation of the phantom may have contributed to error measurements to some extent. Repeated punctures of the phantom may increase the registration error (observed on one occasion) by displacing the internal fiducial or the entire phantom itself. The “vessels” created within the phantom do not have exactly uniform diameters and vary in geometric relationship to each other. Nevertheless, the experiments do permit an estimation of the *overall error magnitude* for the guidance system under motion conditions simulating human respiratory motion. The puncture success rate for 5-mm diameter vessels is somewhat lower than previously presented (19), although an entirely different phantom design was adopted for these experiments. The foam elastomer phantom in the previous trials was abandoned due to the short shelf-life of the ingredi-

ents, which contributed to greater variations in phantom size and shape during curing.

A significant limitation of the current system is the rigid body assumption for the registration process. Simply stated, the liver is assumed to be a rigid structure that uniformly moves in a craniocaudal direction only during respiration. The phantom design for these experiments exhibited a small amount of motion during needle puncture (which could be easily observed), although the mammalian (animal model) and human liver will certainly exhibit significant and complex respiratory related motion. It remains to be determined how significantly the 4.23 mm overall error underestimates the tracking system error margin in vivo. Some research groups are investigating nonrigid registration algorithms that are beyond the scope of this article (20).

This initial experience with the Aurora electromagnetic tracking guidance system suggests that vessels or ducts measuring 5 mm in diameter or less can be successfully punctured in less than 50% of attempts. The reproducibility of this degree of initial puncture accuracy must be assessed in an animal model before a more definitive conclusion regarding the potential clinical efficacy of magnetic tracking-guided needle placement can be reached.

Greater potential for an efficacious role for electromagnetic tracking guidance lies with image-guided biopsies and interventions such as radiofrequency ablation of large liver lesions. In the radiofrequency ablation case, treatment of lesions larger than the prescribed zone of ablation for a given probe can be accomplished by treating overlapping zones or spheres, which would encompass the entire lesion. Given a preoperative CT scan, a software algorithm could generate the necessary overlapping treatment spheres and geometric center of each sphere. Each geometric center would then serve as a target for electromagnetically tracked radiofrequency ablation needle probe placement. Registration of functional imaging data such as positron emission tomography with conventional CT images and magnetic coordinates would facilitate targeting of biopsies or specific alternative therapy to persistently viable tumor tissue visible only with PET imaging.

As we conduct future experiments with the system in a swine model, we are also developing concepts for implanted retrievable devices which would provide multiple internal fiducials, hopefully enhancing the accuracy of the system for liver interventions.

ACKNOWLEDGMENTS

The content of this manuscript does not necessarily reflect the position or policy of the US government. The authors thank Northern Digital Inc for the loan of the Aurora electromagnetic tracking system.

REFERENCES

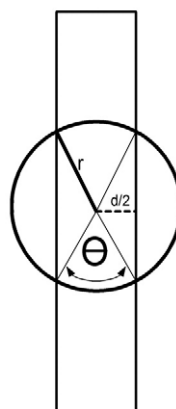
- Rose SC, Behling C, Roberts AC, et al. Main portal vein access in transjugular intrahepatic portosystemic shunt procedures: use of three-dimensional ultrasound to ensure safety. *J Vasc Interv Radiol* 2002; 13:267-273.
- Roizental M, Kane RA, Takahashi J, et al. Portal vein: US guided localization prior to transjugular intrahepatic portosystemic shunt placement. *Radiology* 1995; 196:868-870.
- Kee ST, Rhee JS, Butts K, et al. 1999 Gary J. Becker Young Investigator Award. MR-guided transjugular portosystemic shunt placement in a swine model. *J Vasc Interv Radiol* 1999; 10:529-535.
- Sheppard DG, Moss J, Miller M. Imaging of the portal vein during transjugular portosystemic shunt procedures: a comparison of carbon dioxide and iodinated contrast. *Clin Radiol* 1998; 53:448-450.
- Harman JT, Reed JD, Kopecky KK, et al. Localization of the portal vein for transjugular catheterization: percutaneous placement of a metallic marker with real-time US guidance. *J Vasc Interv Radiol* 1992; 3:545-547.
- Fontaine AB, Verschyl A, Hoffer E, et al. Use of CT-guided marking of the portal vein in creation of 150 transjugular intrahepatic portosystemic shunts. *J Vasc Interv Radiol* 1997; 8:1073-1077.
- Magnetic Tracking Technology. Available online at: www.cs.nps.navy.mil/people/faculty/capps/4473/projects/mag-track/full.html. Accessed September 16, 2003.
- Solomon SB, Magee C, Acker DE, et al. TIPS placement in swine, guided by electromagnetic real-time needle tip localization displayed on previously acquired 3-D CT. *Cardiovasc Intervent Radiol* 1999; 22: 411-414.
- Banovac F, Levy EB, Lindisch D, et al. Feasibility of percutaneous transabdominal portosystemic shunt creation. *Surg Radiol Anat* 2002; 24:217-221.
- Davies S, Hill A, Holmes R, et al. Ultrasound quantitation of respiratory organ motion in the upper abdomen. *Br J Radiol* 1994; 67:1096-1102.
- Cleary K, Stoianovici D, Glossop N, et al. CT-directed robotic biopsy testbed: motivation and concept. *Proc SPIE Med Imaging* 2001; 4319: 231-236.
- The Pivot Alignment Wizard. In NDI 6D Architect Aurora User's Guide, Revision 1.0. Ontario, Canada: Northern Digital Inc, 2003; 55-59.
- Banovac F, Glossop N, Lindisch D, et al. Liver tumor biopsy in a respiring phantom with the assistance of a novel electromagnetic navigation device. Fifth International Conference, Medical Image Computing and Computer Assisted Intervention-MICCAI, Tokyo: Springer, 2002: 200-207.
- Banovac F, Glossop N, Jay M, et al. Feasibility of image-guided abdominal interventions using a novel magnetic position sensing device in an interventional radiology suite. *Computer Assisted Radiology and Surgery (CARS)*, Amsterdam: Elsevier, 2002; 1091.
- Corral G, Cleary K, Tang J, et al. Orientation accuracy of a magnetic tracking device for image-guided interventions. *Computer Assisted Radiology and Surgery (CARS)*, Amsterdam: Elsevier, 2003; 1367.
- Solomon SB, White P Jr, Wiener CM, et al. Three-dimensional CT-guided bronchoscopy with a real-time electromagnetic position sensor: a comparison of two image registration methods. *Chest* 2000; 111:1783-1787.
- Bloch R, Fontaine A, Borsa J, et al. CT-guided transfemoral portocaval shunt creation. *Cardiovasc Intervent Radiol* 2001; 24:106-110.
- Fitzpatrick JM, West JB, Maurer CR Jr. Predicting error in rigid-body point-based registration. *IEEE Trans Med Imaging* 1998; 17:694-702.
- Levy E, Cleary K, Banovac F, et al. Implementation of a magnetic tracking system for accurate puncture needle guidance. Poster presentation at the 27th Annual Meeting of the Society of Cardiovascular and Interventional Radiology; Baltimore, MD, April 2002.
- Davatzikos C, Shen D, Mohamed A, et al. A framework for predictive modeling of anatomical deformations. *IEEE Trans Med Imaging* 2001; 20:836-843.

APPENDIX

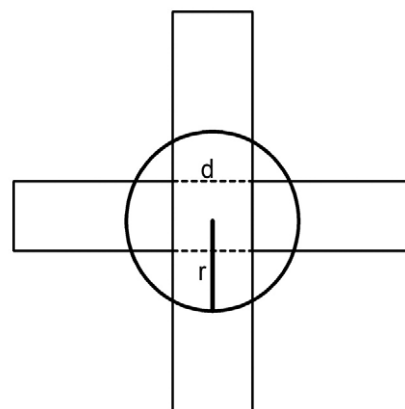
Accuracy Prediction Calculations

Predicted target errors were calculated based on several important assumptions. First, a two-dimensional or planar target area was assumed instead of a target volume to simplify the mathematical calculations. Second, the predicted accuracy is expressed as a mean of the likelihood of successful puncture of the smallest and most difficult puncture target (perpendicular target vessel case) and the largest successful target area (parallel target vessel case).

Parallel Vessel Case



Perpendicular Vessel Case



In both the parallel and perpendicular cases, the zone of possible guided punctures is defined by the area of a circle whose radius is the sum of the system errors and whose center point represents the selected puncture target.

In the parallel vessel case, the successful puncture target area is bounded by the walls of the two vessels (solid black lines) and a small portion of the circumference of the circle which defines all of the possible guided punctures. The probability of successful two-vessel puncture in the target area is given by the ratio of the sum of the areas of two circle sectors (defined by radius r and sector angle θ) and two triangles (short leg r and height $d/2$) divided by the area of the circle of possible punctures.

To calculate the area of one of the circle sectors, the angle θ of the sector must be determined. If we can calculate the size of the angle θ , we can multiply the area of the circle by the fraction

$$\theta/360$$

to figure out the area of a single sector of the circle.

Using the equation relating the legs of a *triangle* in which two legs constitute the boundaries of the *sector*;

$$B^2 = A^2 + C^2 - (2AC)(\cos \Theta)$$

Solving for θ requires the length of the side *opposite* the angle (in this case, the diameter of the vessel; d), and the length of the other two legs (each is equal to the radius of the circle; r).

Solving for θ

$$\Theta = \cos^{-1} [(d^2 - 2r^2)/2r]$$

So the area of successful puncture represented by *one* of the circle sectors is

$$= \frac{\cos^{-1} [(d^2 - 2r^2)/2r] \pi r^2}{360}$$

Now multiplying by two for the *two* sector contribution and the area of the entire circle defined by the sum of errors radius

$$= \frac{\cos^{-1} [(d^2 - 2r^2)/2r] \pi r^2}{180}$$

To determine the area contribution of each *triangle*, the larger triangle must be bisected into two right triangles in which the common leg of the two right triangles is equal to one half the diameter of the vessel. The other known leg length is equal to the radius of the circle. Therefore by Pythagorean Theorem the length of the unknown leg X is given by

$$X^2 = (d/2)^2 + r^2$$

However, X must be doubled to provide the *entire* length of the base of the larger triangle (sum of the two right triangles).

$$2X = 2\sqrt{((d/2)^2 + r^2)}$$

Now the area of the entire triangle is given by the formula (one half the length of the leg $2X$ times the vertical height $d/2$):

$$A = \frac{d/2 + 2\sqrt{((d/2)^2 + r^2)}}{2}$$

This fraction must be multiplied by two to give the total area represented by the sum of the areas of the two identical triangles. Finally, the likelihood of a successful simultaneous puncture of two parallel vessels is expressed by the combined equation:

$$\frac{1}{\pi r^2} * \left[\frac{\cos^{-1} [(d^2 - 2r^2)/2r] \pi r^2}{180} + d/2 + 2\sqrt{((d/2)^2 + r^2)} \right]$$

Analysis for the perpendicular vessel case is relatively simple: the area A of successful puncture is defined by a square whose side is defined by the diameter of the target vessel d ;

$$A = d^2$$

And the area of the circle representing all puncture attempts on a point target whose radius r equals the total guidance system error is defined as:

$$A(\text{circle}) = \pi r^2$$

Therefore, the probability of a successful guided two vessel puncture in the case of perpendicular vessels is given by:

$$d^2 / \pi r^2$$